Electronic Supplementary Material (ESI) for Materials Advances.

Porous Ionic Liquids: Beyond the Bounds of Free Volume in a Fluid Phase

Jocasta Avila, Ryan Clark, Agilio Padua, and Margarida Costa Gomes*

Laboratoire de Chimie de l'ENS Lyon, CNRS and Université de Lyon, 46 allée d'Italie, 69364 Lyon, France

E-mail: margarida.costa-gomes@ens-lyon.fr

Supplementary Information

Materials

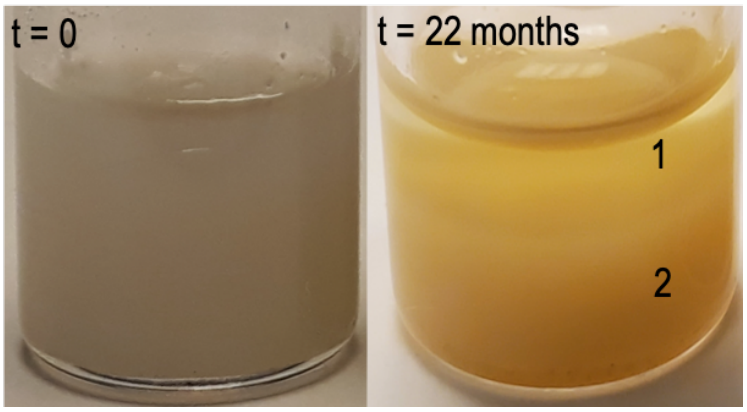

Figure S1: $[P_{6,6,6,14}][NTf_2]$+ZIF-8 (5% w/w) suspension at (left) $t = 0$, right after preparation and (right) after 22 months. Two phases, 1 and 2, are observed in the suspension only after 22 months.

Table S1: Solids abbreviation and nomenclature

Abbreviation	Nomenclature
	Metal organic frameworks (MOFs)
Al(fum)(OH)	aluminium-based fumarate framework
CAU-10-H	aluminium isophthalate-based MOF - $[Al(OH)(benzene{-}_{1,3}{-}dicarboxylate)]{\cdot}nH_2O$
CD-MOF-1	cubic γ-cyclodextrin-based MOF
$Cu(QC)_2$	copper-based quinoline-5-carboxylate MOF
HKUST-1	copper-based benzene-1,3,5-tricarboxylate framework
OPOSS-HKUST-1	copper-based benzene-1,3,5-tricarboxylate framework surface fictionalized with silsesquioxane(OPOSS)
MIL-101(Cr)@xPDMS	chromium-based MOF - $Cr_3O(OH)(H_2O)_2(bdc)_3$, bdc = 1,4-benzenedicarboxylate - surface polymerized with PDMS
MIL-53	ferrous-based MOF - $Fe(OH)(O_2C{-}C_6H_4{-}CO_2)$
MOF-801	zirconium-based MOF - $Zr_6O_4(OH)_4(fumarate)_6$
SIFSIX-3-Zn	zinc-based hexafluorosilicate framework
SIFSIX-3-Cu	copper-based hexafluorosilicate framework
UiO-66	zirconium-based MOF - $[Zr_6O_4(OH)_4]$ clusters and 1,4-benzodicarboxylic acid struts
UiO-66(185)@xPDMS	UiO-66(185 nm particle diameter) surface polymerized with PDMS
UiO-66(484)@xPDMS	UiO-66(484 nm particle diameter) surface polymerized with PDMS
UiO-66-NH_2	UiO-66 amino functionalized
UiO-66-NH_2@xPDMS	UiO-66 amino functionalized and surface polymerized with PDMS
UiO-66-Br_2@xPDMS	UiO-66 bromineted and surface polymerized with PDMS
ZIF-7	zinc-based benzimidazolate framework
ZIF-8	zinc-based zeolitic imidazolate framework - $Zn(MeIm)_2$, MeIm = 2-methylimidazolate
ZIF-8-g-BPEI(153)	Branched polyethyleneimine (BPEI) grafted ZIF-8 - 153 nm particle diameter
ZIF-8-g-BPEI(530)	Branched polyethyleneimine (BPEI) grafted ZIF-8 - 530 nm particle diameter
HPMo@ZIF-8(100-150)	zinc-based zeolitic imidazolate framework surface functionalized with phophomolybdic acid
ZIF-67	cobalt-based zeolitic imidazolate framework - $Co(Hmim)_2$, Hmim = 2-methylimidazolate
ZIF-67-IDip	ZIF-67 surface modified with IDip (1,3-bis(2,6-diisopropylphenyl)imidazole-2-ylidene)
ZIF-67-IMes	ZIF-67 surface modified with IMes (1,3-bis(2,4,6-trimethylphenyl)imidazole-2-ylidene)
ZIF-90	zinc-based zeolitic imidazole-2-Carboxaldehyde framework
	Zeolites
Silicate-1	silicium-based hydrophobic zeolite
ZSM-5	aluminosilicate zeolite - $Na_nAl_nSi_{96-n}O_{192}{\cdot}16H_2O$ $(0 < n < 27)$
H-ZSM-5	hierarchical aluminosilicate zeolite
Zeolite(Sigma)	
Zeolite 5A	calcium aluminosilicate - $Ca_{4,5}[(AlO_2)_{12}(SiO_2)_{12}]\cdot nH_2O$
Zeolite 13X	sodium aluminosilicate - $Na_{86}[(AlO_2)_{86}(SiO_2)_{106}]\cdot H_2O$
Zeolite AgA	Ag-exchanged zeolite A ($[(Na_{12}(H_2O)_{27}]_8[Al_{12}Si_{12}O_{48}]_8$)
MCM-22	layered nanosheets zeolite
	Porous organic polymers (MOPs)
PAF-1	tetrahedral carbon atoms connected by biphenyl group
	Porous organic cages (POCs)
CC3-R	1,3,5-Triformylbenzene Cyclohexane-1,2-diamine(R,R) based POC
CC3-S	1,3,5-Triformylbenzene Cyclohexane-1,2-diamine(S,S) based POC
CC3-R/S_{xnm}	CC3-R:CC3-S (1:1), x = 600, 630, 720, 940 and 1200 nm
CC15-S	1,3,5-triacetylbenzene Cyclohexane-1,2-diamine(S,S) based POC
CC19-S	2-Hydroxy-1,3,5-benzenetricarbaldehyde Cyclohexane-1,2-diamine(S,S) based POC
CC3-R/CC15-$S_{17000nm}$	CC3-R:CC15-S (1:1), 1700 nm
CC3-R/CC19-$S_{17000nm}$	CC3-R:CC19-S (1:1), 1700 nm
	Covalent organic framework (COF)
COF-300(200)	3D imine-linked covalent organic framework; 200 nm
	Nanocarbon
HCNS	holow carbon nanospheres
PIL@HCS	holow carbon spheres (HCS) surface functionalized with polymerized 1-vinyl-3-butyronitrile imidazolium bromide ionic liquid (PIL)

Table S2: Solvents abbreviation and nomenclature

Abbreviation	Nomenclature
	Molecular solvents
Glycol	1,2-ethanediol
Glycol:mIm (3:2)	1,2-ethanediol:2-methylimidazole (3:2)
Mesitylene	1,3,5-trimethylbenzene
	Polymers and oils
AR20	silicone oil AR20 or polyphenyl-methylsiloxane
Fomblin Y oil(60cst)	Perfluoropolyether Y06 - PFPE2.4k ($CF_3-[(OC(CF_3)FCF_2)_m-(OCF_2)_n]OCF_3$)
Krytox oil(177cst)	Perfluoropolyether - PFPE ($F-(CF(CF_3)-CF_2-O)_n-CF_2CF_3$)
PDMS	polydimethylsiloxane
PDMS4k	polydimethylsiloxane, trimethylsiloxy terminated ($M_w = 4000 g\,mol^{-1}$)
PEO500	poly(ethylene glycol) dimethyl ether with ($M_w = 500 g\,mol^{-1}$)
BPEI	branched polyethyleneimine
	Ionic liquids
[$Aliquant_{336}$][Cl]	methyltrioctylammonium chloride
[Bpy][NTf_2]	N-butyl pyridinium bis(trifluoromethyl sulfonyl)imide
[Bpy][BF_4]	N-butyl pyridinium tetrafluoroborate
[Bmim][NTf_2]	1-butyl-3-methylimidazolium bis(trifluoromethylsulfonylamide)
[Emim][NTf_2]	1-ethyl-3-methylimidazolium bis(trifluoromethylsulfonylamide)
[DBU−PEG][NTf_2]	8,8'-(3,6-dioxaoctane-1,8-diyl)bis(1,8-Diazabicyclo(5.4.0)undec-7-en-8-ium) bis(trifluoromethanesulfonyl)imide
[Hpy][NTf_2]	N-hexylpyridinium bis(trifluoromethylsulfonylamide)
[$P_{4,4,4,2}$][Suc]	tributyltetraethylphosphonium chloride
[$P_{4,4,4,4}$][OAc]	tetrabutylphosphonium acetate
[$P_{4,4,4,4}$][Lev]	tetrabutylphosphonium levulinate
[$P_{4,4,4,8}$][Cl]	tributyltetraoctylphosphonium chloride
[$P_{6,6,6,14}$][Cl]	trihexyltetradecylphosphonium chloride
[$P_{6,6,6,14}$][Br]	trihexyltetradecylphosphonium bromine
[$P_{6,6,6,14}$][NTf_2]	trihexyltetradecylphosphonium bis(trifluoromethylsulfonylamide)
[$M2070$][PSS]	polyether amonium (M2070) poly(4-styrenesulfonate) (PSS)
[$C_6(bmim)_2$][NTf_2]$_2$	1,6-bis (3-buthylimidazolium-1-yl) hexane bis(trifluoromethylsulfonyl)amide
[BEMA][NTf_2]	benzyl(ethyl)dimethyl ammonium bis(trifluoromethanesulfonyl)imide
[MBPy][NTf_2]	p-methyl-N-buthyl pyridinium bis(trifluoromethyl sulfonyl)imide
[TBPy][NTf_2]	t-buthyl pyridinium bis(trifluoromethyl sulfonyl)imide
[BBIm][NTf_2]	1,3-buthylimidazolium bis(trifluoromethyl sulfonyl)imide
[$N_{8,8,8,1}$][Cl]	trioctylmethylammonium chloride
BAR^F	3-(3-(4-formylphenoxy propyl)-1-methyl-1H-imidazol-3-ium

Dissolution calorimetry

The heat of wettability of MOFs (ZIF-8 and HKUST-1) in the ILs ($[P_{6,6,6,14}][NTf_2]$ and $[P_{6,6,6,14}][Cl]$) were measured using a 20 mL micro solution calorimeter housed in a TAM IV thermostat from TA Instruments in a dynamic mode. The experiments were performed at 323 K, mechanically stirred at 90 rpm and the quantities of MOF and IL were determined gravimetrically using a Mettler Toledo New Classic MS balance with an accuracy of ±0.01 mg (Table S3). At each experiment, the calorimeter measuring cell was assembled following 4 steps: (1) three cylindrical cartridges, composed of two walls and one base cap, containing the solid sample were loaded into the plunger in the underside of the ampoule lid of the calorimeter, (2) a gold stirrer combined with a stainless steel turbine and propeller was assembled in the ampoule lid at 2 mm from the ampoule bottom, (3) the stainless steel ampoule filled with the IL (about 15 mL) was connected to the lid and, finally, (4) the calorimeter was lowered slowly into the TAM IV thermostat respecting three equilibration positions to avoid damaging the sensor. An ampoule filled with water, same weight as the IL in the measuring cell, was used as a reference cell. After achieving temperature equilibrium and a constant baseline, standard deviation about 200–500 nW, a full dynamic calibration was performed. A initial baseline was acquired during ≈15 min to achieve absolute value of slope less than 500 nW h^{-1} and standard deviation less than 100 nW. The cartridges were then injected sequentially into the stirred dispersion medium within the sample ampoule by manually pressing the injector. After each injection, the heat flow signal is collect until the baseline achieve the stability conditions as stated before (Figure S3). A final baseline was collected before ending the experiment.

The heat effect of the addition of the empty cartridge and of the solid in the IL or IL/MOF mixture (after the addition of the first cartridge containing solid) were obtained by the integration of each peak, heat flow *vs.* time, using the integration against a baseline tool of the TAM Assistant software. The energy related to solid dispersion in the IL was obtained by subtracting the heat effect promoted by the empty cartridge from the total heat effect of the solid+cartridge at each experiment. In the case of ZIF-8 dispersed in $[P_{6,6,6,14}][NTf_2]$, a baseline correction was necessary due to the non complete recover of

the initial heat flow. All the adjustments and integration values are depicted in Figures S5-S7 and Tables S4-S5.

Table S3: Ampoule (m_{H_2O} and m_{IL}) and cartridge (m_I, m_{II} and m_{III}) composition of the micro solution calorimeter.

	Reference cell	Measuring cell			
Exp. #	m_{H_2O}/ g	m_{IL}/ g	m_I(MOF)/ mg	m_{II}(MOF)/ mg	m_{III}(MOF)/ mg
			$[P_{6,6,6,14}][NTf_2]$ + ZIF-8		
1	15.46679	15.47268	0.0	4.18	5.54
2	15.46679	15.47672	0.0	3.91	6.12
			$[P_{6,6,6,14}][Cl]$ + ZIF-8		
1	15.68113	15.50983	3.56	5.07	0.0
2	15.43428	15.43098	0.0	3.53	5.43
			$[P_{6,6,6,14}][NTf_2]$ + HKUST-1		
1	15.46679	15.47268	0.0	4.16	6.11

Table S4: Heat effect of metallic cartridge and the solid in contact with the IL. Peaks I, II and III corresponds to the samples m_I, m_{II} and m_{III} presented in S3. The heat values of Peaks II and III were obtained by subtracting the blank of each experiment from the integral of each peak (Figures S4, S5 and S6).

	Measuring cell					
Exp. #	Peak I/ mJ	Peak II/ mJ	Peak III/ mJ	Peak I/ $J\,g^{-1}$	Peak II/ $J\,g^{-1}$	Peak III/ $J\,g^{-1}$
	$[P_{6,6,6,14}][NTf_2]$ + ZIF-8					
1	19	501	564	-	120	102
2	20	460	615	-	118	101
	$[P_{6,6,6,14}][Cl]$ + ZIF-8					
1	3174	3987	29	892	786	-
2	17	2873	4662	-	814	859
	$[P_{6,6,6,14}][NTf_2]$ + HKUST-1					
1	20	-334	-337	-	-80	-55

Table S5: Asymmetric least squares smoothing baseline parameters for the $[P_{6,6,6,14}][NTf_2]$ + ZIF-8 calorimetric peaks.

Exp. #	Peak	Asymmetric factor	Threshold	Smoothing factor	Iteraction #
		$[P_{6,6,6,14}][NTf_2]$ + ZIF-8			
1	Blank 1	-	-	-	-
1	S1	0.001	0.001	9	10
1	S2	0.001	0.001	8	10
2	Blank 2	-	-	-	-
2	S3	0.001	0.001	8	10
2	S4	0.001	0.001	9	10

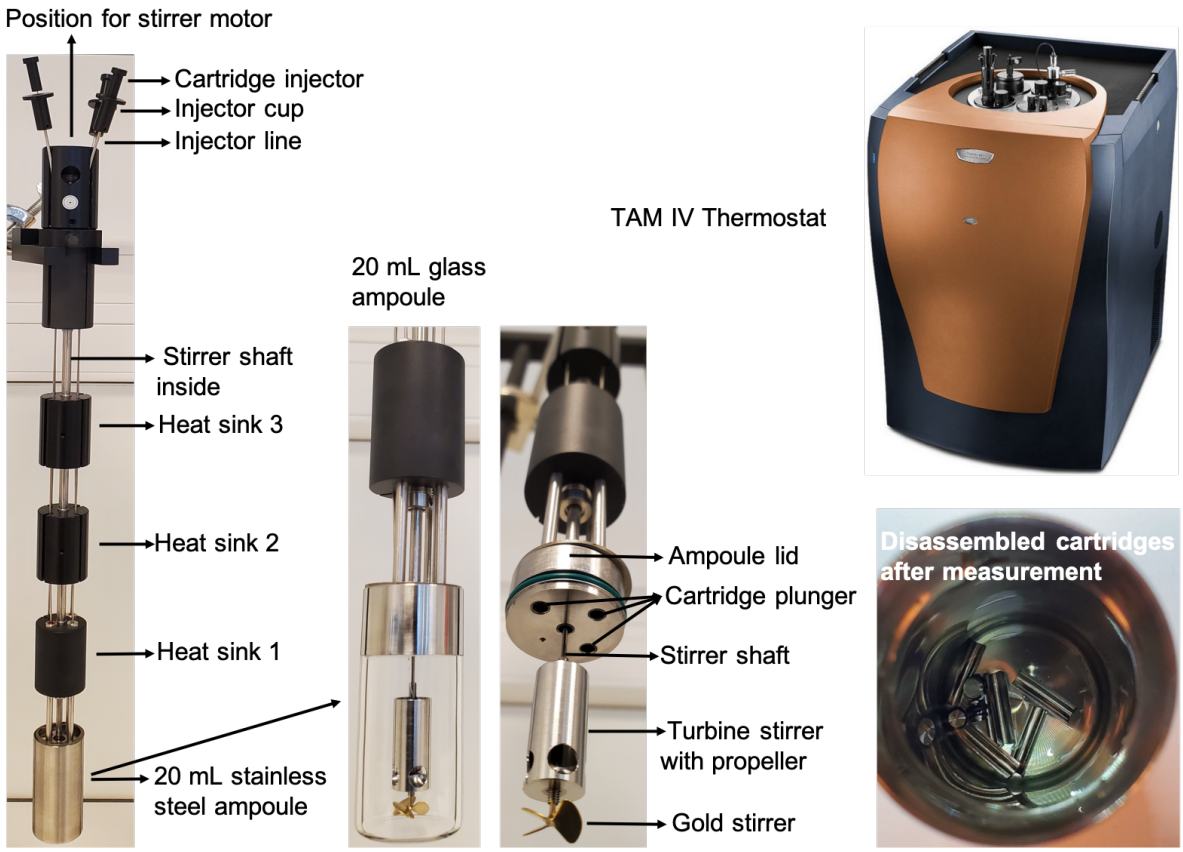

Figure S2: Micro solution calorimeter components housed in a TAM IV thermostat. A 20 mL glass ampoule is also presented in the picture only to show the internal part of of the sample ampoule in a assembled calorimeter. After each measurement, the three disassembled cartridges are recovered from the solid-liquid mixture.

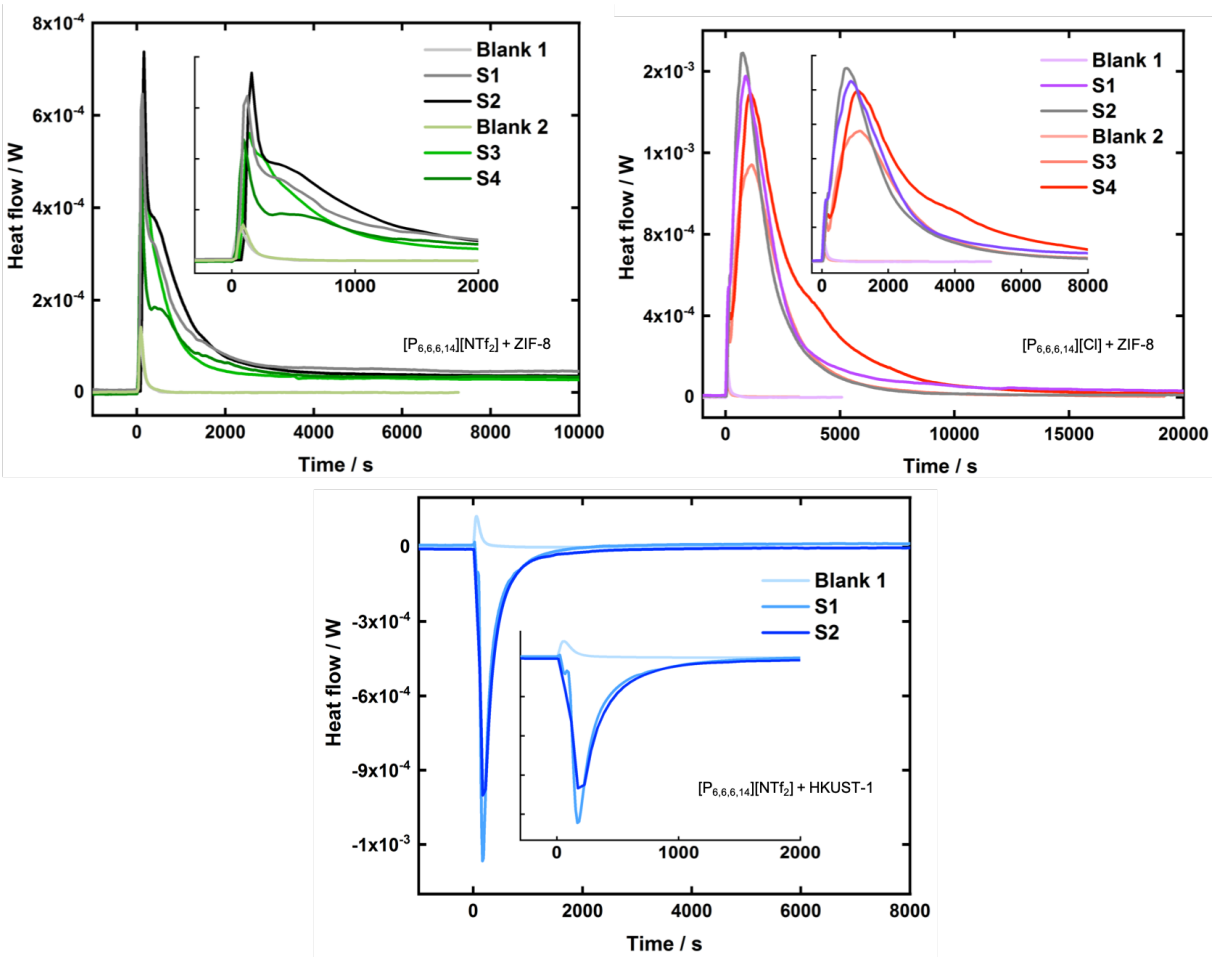

Figure S3: Heat change caused by the addition of ZIF-8 in (top left) $[P_{6,6,6,14}][NTf_2]$ and (top right) $[P_{6,6,6,14}][Cl]$ and of (bottom) HKUST-1 in $[P_{6,6,6,14}][NTf_2]$. The heat effect of the empty metallic cartridges are also depicted in each graph. The inner graphs highlight the line shape at shorter time.

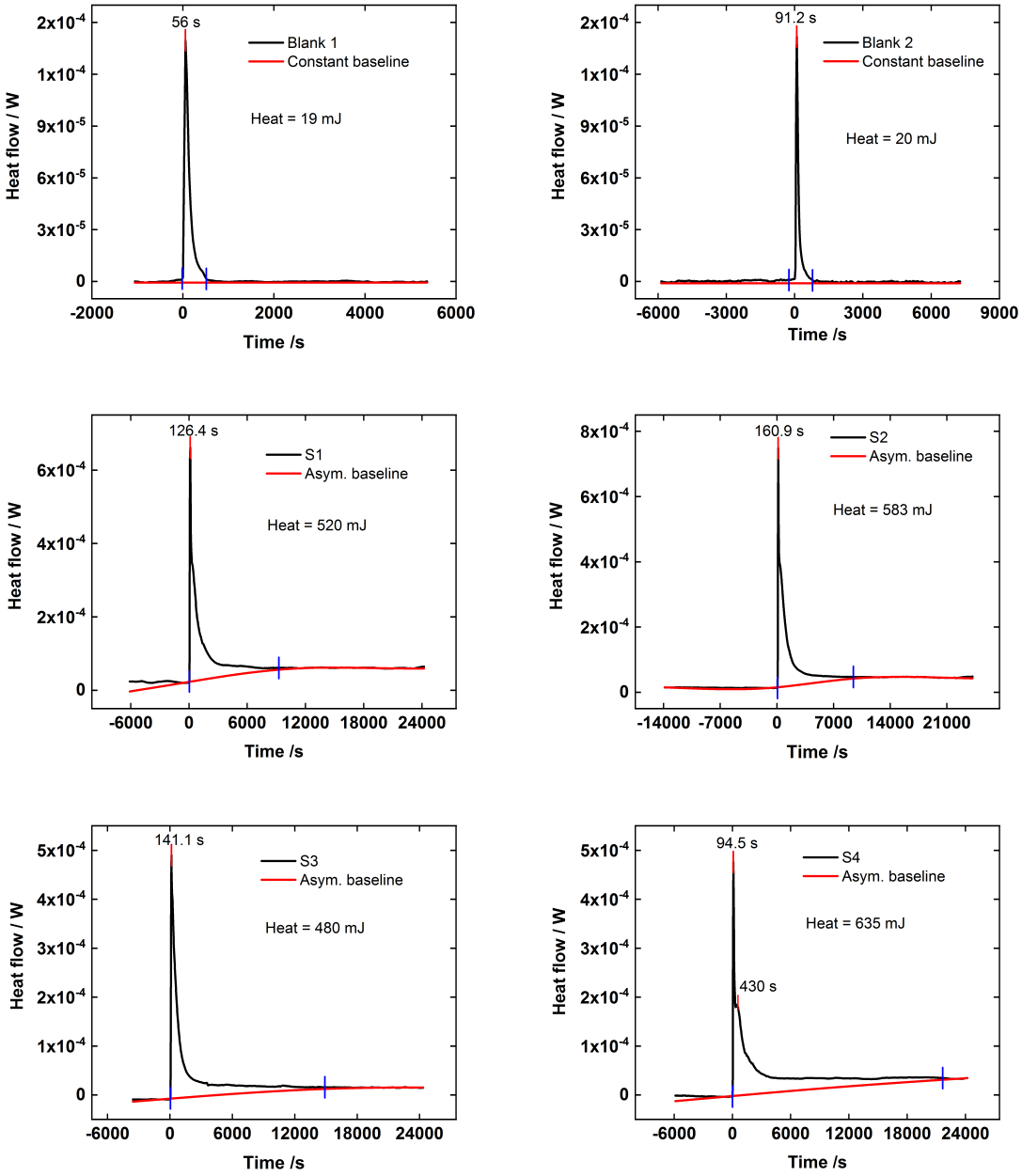

Figure S4: Integration procedure of the individual heat signals of the $[P_{6,6,6,14}][NTf_2]$+ZIF-8 calorimetric experiments. The asymmetric least squares smoothing baseline (horizontal red lines), the integration region (vertical blue lines) and the peak center (vertical red lines) are also depicted in each graph. The time scale was shifted accordingly to set the beginning of each heat signal as zero, which allow us to better see the time length of each peak.

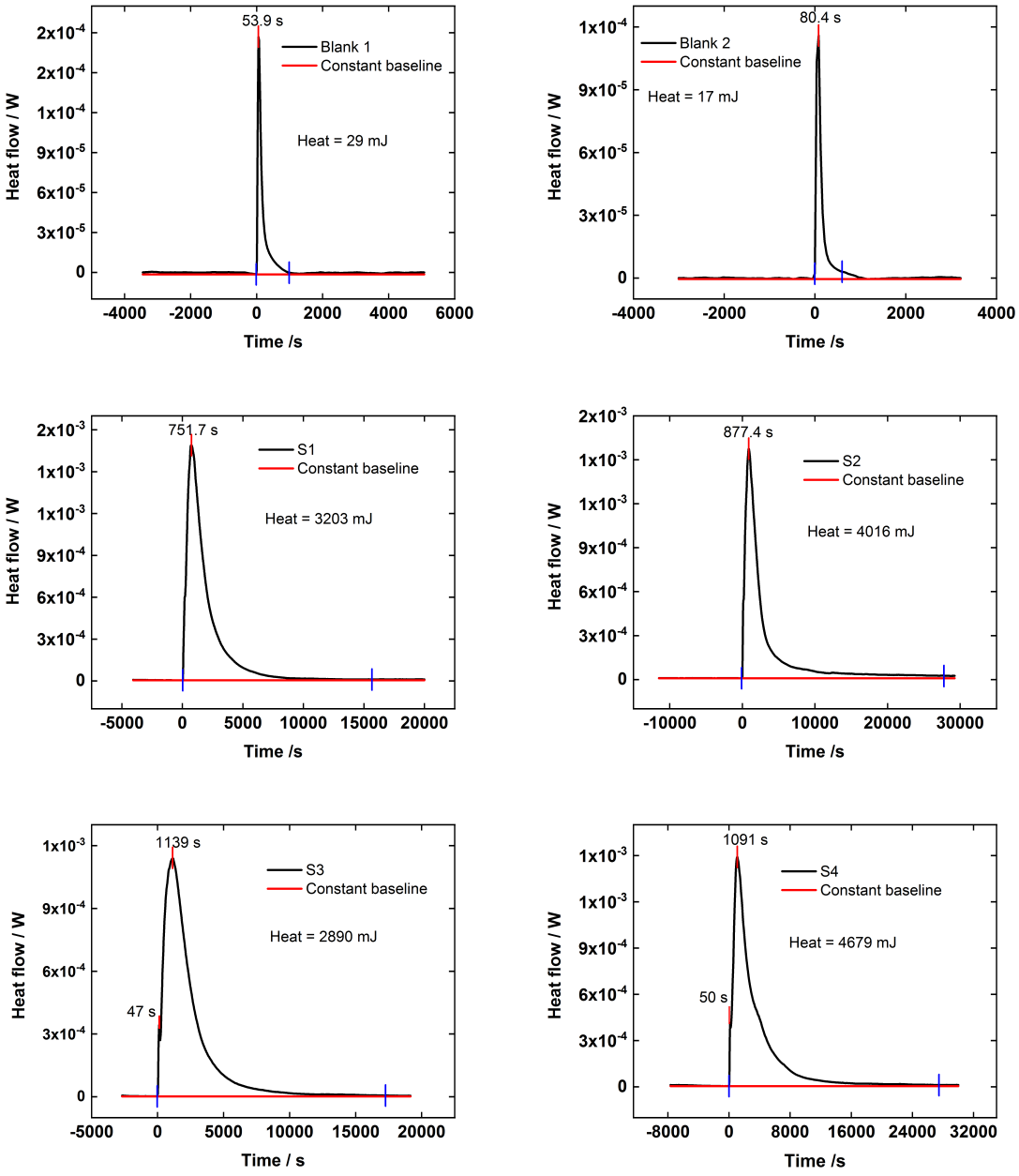

Figure S5: Integration procedure of the individual heat signals of the $[P_{6,6,6,14}][Cl]$+ZIF-8 calorimetric experiments. The constant baseline (horizontal red lines), the integration region (vertical blue lines) and the peak center (vertical red lines) are also depicted in each graph. The time scale was shifted accordingly to set the beginning of each heat signal as zero, which allow us to better see the time length of each peak.

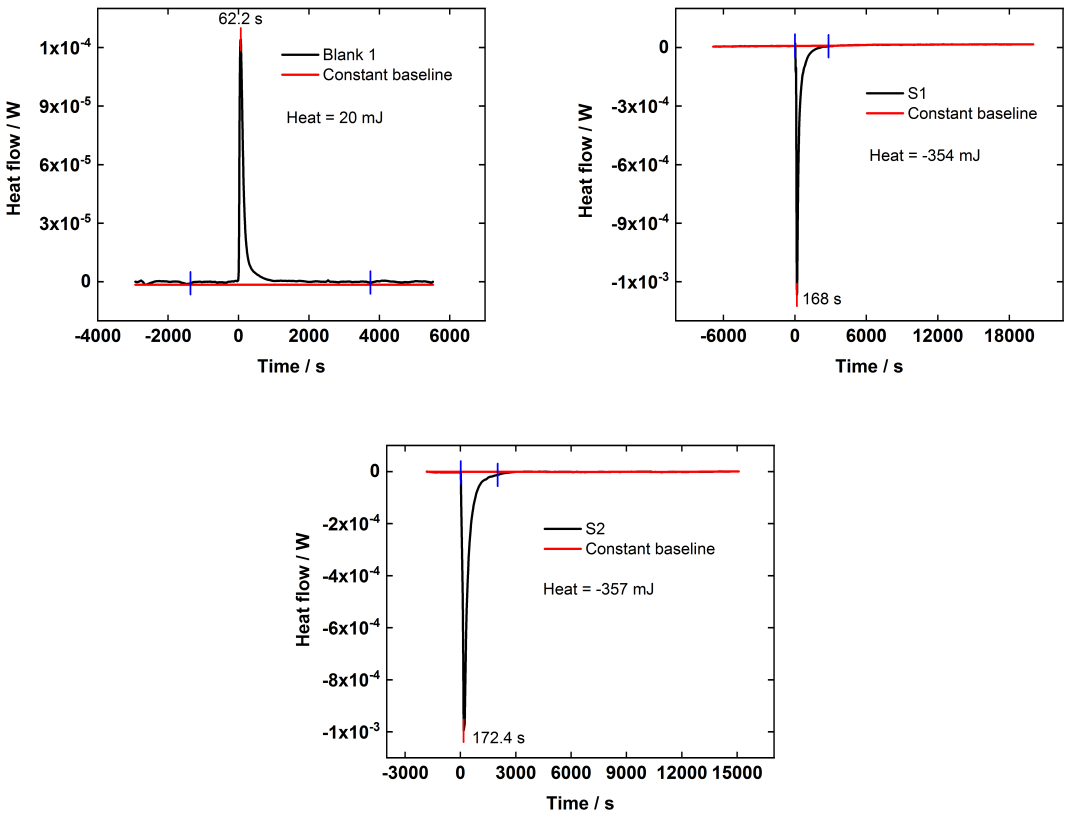

Figure S6: Integration procedure of the individual heat signals of the $[P_{6,6,6,14}][NTf_2]$+HKUST-1 calorimetric experiments. The constant baseline (horizontal red lines), the integration region (vertical blue lines) and the peak center (vertical red lines) are also depicted in each graph. The time scale was shifted accordingly to set the beginning of each heat signal as zero, which allow us to better see the time length of each peak.

Molecular simulation

In the molecular simulations the force field used for the ionic liquids was the CL&Pol force field,[1] and the flexible AMBER model of[2] was used for the ZIF-8.

The Drude particle methodology for polarisation and Lennard-Jones parameter scaling of[1] was used, with polarisabilities of the ionic liquid and 2-methylimidazole in ZIF-8 taken from,[3] and zinc taken from[4] The polarisabilities of the zinc and 2-methylimidazole groups were scaled according to the model of the excess electron.[5]

Simulation boxes were built using the Packmol[6] and fftool[7] packages. Drude particles were added and Lennard-Jones parameters scaled using the polarizer and scaleLJ scripts provided with the CL&Pol force field.[1,8]

The ZIF-8 unit cell was taken from the CCDC[9] and a periodic slab of ZIF-8 crystal was generated which was periodic in nature in the x and y dimensions, with 3 unit cells along each dimension (51 Å length). Along the z direction 2 unit cells were built, and unsaturated Zn atoms saturated with methylimidazole groups. The dangling bonds on the methylimidazole groups were saturated with hydrogen atoms, the charge of which was adjusted to ensure the ZIF-8 slab was neutral.[10]

Simulations were run in LAMMPS using a time step of 1 fs.[11] A cutoff of 12 Å was used for Lennard-Jones potentials, with tail corrections for energy and pressure. The particle-particle particle-mesh method was used to evaluate electrostatic energies with a relative accuracy of 1×10^{-5}. Bonds terminating in hydrogen were constrained using the SHAKE algorithm. All simulations were thermostatted at 353 K and 5 bar using the tg-NH thermostat and barostat, with a Drude particle temperature of 1 K.

Boxes of ZIF-8 and ionic liquids were equilibrated separately for 10 ns, then annealed and equilibrated for a further 10 ns in an isothermal–isobaric ensemble. A 10 ns NVT production run was then performed. Figures were generated in VMD.[12]

References

(1) Goloviznina, K.; Canongia Lopes, J. N.; Costa Gomes, M.; Pádua, A. A. H. Transferable, Polarizable Force Field for Ionic Liquids. Journal of Chemical Theory and Computation **2019**, 15, 5858–5871.

(2) Zheng, B.; Sant, M.; Demontis, P.; Suffritti, G. B. Force Field for Molecular Dynamics Computations in Flexible ZIF-8 Framework. The Journal of Physical Chemistry C **2012**, 116, 933–938.

(3) Heid, E.; Szabadi, A.; Schröder, C. Quantum mechanical determination of atomic polarizabilities of ionic liquids. Physical Chemistry Chemical Physics **2018**, 20, 10992–10996.

(4) Schwerdtfeger, P.; Nagle, J. K. 2018 Table of static dipole polarizabilities of the neutral elements in the periodic table. Molecular Physics **2019**, 117, 1200–1225.

(5) Bernardes, C. E. S.; Shimizu, K.; Lopes, J. N. C.; Marquetand, P.; Heid, E.; Steinhauser, O.; Schröder, C. Additive polarizabilities in ionic liquids. Physical Chemistry Chemical Physics **2016**, 18, 1665–1670.

(6) Martinez, L.; Andrade, R.; Birgin, E. G.; Martínez, J. M. PACKMOL: A package for building initial configurations for molecular dynamics simulations. Journal of Computational Chemistry **2009**, 30, 2157–2164.

(7) Pádua, A. A. fftool V1.0.0. 2015; https://www.zenodo.org/record/18618.

(8) Goloviznina, K.; Padua, A. polil. 2021; https://github.com/agiliopadua/clandpol.

(9) Morris, W.; Stevens, C. J.; Taylor, R. E.; Dybowski, C.; Yaghi, O. M.; Garcia-Garibay, M. A. NMR and X-ray Study Revealing the Rigidity of Zeolitic Imidazolate Frameworks. The Journal of Physical Chemistry C **2012**, 116, 13307–13312.

(10) Costa Gomes, M.; Pison, L.; Červinka, C.; Padua, A. Porous Ionic Liquids or Liquid Metal–Organic Frameworks? Angew. Chemie - Int. Ed. **2018**, 57, 11909–11912.

(11) Plimpton, S. Fast parallel algorithms for short-range molecular dynamics. Journal of Computational Physics **1995**, 117, 1–19.

(12) Humphrey, W.; Dalke, A.; Schulten, K. VMD: Visual molecular dynamics. Journal of Molecular Graphics **1996**, 14, 33–38.